



HAL
open science

Single-Cell RNAseq Profiling of Human $\gamma\delta$ T Lymphocytes in Virus-Related Cancers and COVID-19 Disease

Juan Pablo Cerapio, Marion Perrier, Frédéric Pont, Marie Tosolini, Camille Laurent, Stephane Bertani, Jean-Jacques Fournie

► **To cite this version:**

Juan Pablo Cerapio, Marion Perrier, Frédéric Pont, Marie Tosolini, Camille Laurent, et al.. Single-Cell RNAseq Profiling of Human $\gamma\delta$ T Lymphocytes in Virus-Related Cancers and COVID-19 Disease. *Viruses*, 2021, 13 (11), pp.2212. 10.3390/v13112212 . hal-03413561

HAL Id: hal-03413561

<https://hal.science/hal-03413561>

Submitted on 3 Nov 2021

HAL is a multi-disciplinary open access archive for the deposit and dissemination of scientific research documents, whether they are published or not. The documents may come from teaching and research institutions in France or abroad, or from public or private research centers.




L'archive ouverte pluridisciplinaire **HAL**, est destinée au dépôt et à la diffusion de documents scientifiques de niveau recherche, publiés ou non, émanant des établissements d'enseignement et de recherche français ou étrangers, des laboratoires publics ou privés.



Distributed under a Creative Commons Attribution 4.0 International License

Article

Single-Cell RNAseq Profiling of Human $\gamma\delta$ T Lymphocytes in Virus-Related Cancers and COVID-19 Disease

Juan Pablo Cerapio ^{1,2,3,4,5,*}, Marion Perrier ^{1,2,3,4,5}, Frédéric Pont ^{1,2,3,4,5} , Marie Tosolini ^{1,2,3,4,5} ,
Camille Laurent ^{1,2,3,4,5,6,7}, Stéphane Bertani ^{2,8}  and Jean-Jacques Fournie ^{1,2,3,4,5,6,*,†}

¹ Centre de Recherches en Cancérologie de Toulouse, Inserm UMR 1037, 31037 Toulouse, France; marion.perrier@inserm.fr (M.P.); frederic.pont@inserm.fr (F.P.); marie.tosolini@inserm.fr (M.T.); camille.laurent@inserm.fr (C.L.)

² Toulouse University, 31062 Toulouse, France; stephane.bertani@ird.fr

³ CNRS UMR 5071, 31024 Toulouse, France

⁴ Institut Universitaire du Cancer-Oncopole de Toulouse, 31100 Toulouse, France

⁵ Laboratoire d'Excellence 'TOUCAN-2', 31037 Toulouse, France

⁶ Institut Carnot Lymphome CALYM, 75014 Paris, France

⁷ Centre Hospitalier Universitaire, 31300 Toulouse, France

⁸ PHARMADEV, IRD UMR 152, 31062 Toulouse, France

* Correspondence: juan-pablo.cerapio-arroyo@inserm.fr (J.P.C.); jean-jacques.fournie@inserm.fr (J.-J.F.)

† Lead contact.

Abstract: The detailed characterization of human $\gamma\delta$ T lymphocyte differentiation at the single-cell transcriptomic (scRNAseq) level in tumors and patients with coronavirus disease 2019 (COVID-19) requires both a reference differentiation trajectory of $\gamma\delta$ T cells and a robust mapping method for additional $\gamma\delta$ T lymphocytes. Here, we incepted such a method to characterize thousands of $\gamma\delta$ T lymphocytes from ($n = 95$) patients with cancer or adult and pediatric COVID-19 disease. We found that cancer patients with human papillomavirus-positive head and neck squamous cell carcinoma and Epstein–Barr virus-positive Hodgkin's lymphoma have $\gamma\delta$ tumor-infiltrating T lymphocytes that are more prone to recirculate from the tumor and avoid exhaustion. In COVID-19, both TCRV $\gamma 9$ and TCRV $\gamma non9$ subsets of $\gamma\delta$ T lymphocytes relocate from peripheral blood mononuclear cells (PBMC) to the infected lung tissue, where their advanced differentiation, tissue residency, and exhaustion reflect T cell activation. Although severe COVID-19 disease increases both recruitment and exhaustion of $\gamma\delta$ T lymphocytes in infected lung lesions but not blood, the anti-IL6R therapy with Tocilizumab promotes $\gamma\delta$ T lymphocyte differentiation in patients with COVID-19. PBMC from pediatric patients with acute COVID-19 disease display similar $\gamma\delta$ T cell lymphopenia to that seen in adult patients. However, blood $\gamma\delta$ T cells from children with the COVID-19-related multisystem inflammatory syndrome are not lymphodepleted, but they are differentiated as in healthy PBMC. These findings suggest that some virus-induced memory $\gamma\delta$ T lymphocytes durably persist in the blood of adults and could subsequently infiltrate and recirculate in tumors.

Keywords: human; gammadelta; lymphocyte; tumor; COVID-19; transcriptome; single cell; differentiation; trajectory



Citation: Cerapio, J.P.; Perrier, M.; Pont, F.; Tosolini, M.; Laurent, C.; Bertani, S.; Fournie, J.-J. Single-Cell RNAseq Profiling of Human $\gamma\delta$ T Lymphocytes in Virus-Related Cancers and COVID-19 Disease. *Viruses* **2021**, *13*, 2212. <https://doi.org/10.3390/v13112212>

Academic Editor: Eric Champagne

Received: 14 September 2021

Accepted: 20 October 2021

Published: 3 November 2021

Publisher's Note: MDPI stays neutral with regard to jurisdictional claims in published maps and institutional affiliations.



Copyright: © 2021 by the authors. Licensee MDPI, Basel, Switzerland. This article is an open access article distributed under the terms and conditions of the Creative Commons Attribution (CC BY) license (<https://creativecommons.org/licenses/by/4.0/>).

1. Introduction

Efficient protection against viruses and cancers requires innate and adaptive immunity. Due to their ontogeny, antigen recognition mode, and effector functions, $\gamma\delta$ T lymphocytes are involved in both types of immune defense [1]. As a result, $\gamma\delta$ T cells are activated by a wide array of viral infections as well as by many different types of cancer. Human CD4[−]CD8[−] $\gamma\delta$ T lymphocytes express either TCRV $\delta 2$ or TCRV $\delta 1/3$ chains prominently paired with TCRV $\gamma 9$ or TCRV $\gamma 2/3/4/5/8$ (TCRV $\gamma non9$), respectively. The TCRV $\gamma 9$ V $\delta 2$ $\gamma\delta$ T cells are prominently circulating lymphocytes specifically reactive to phosphoantigen-sensing butyrophilins while TCRV $\gamma non9$ $\gamma\delta$ T cells are mostly tissular and recognize

more diversified antigens. Upon antigen activation, both subtypes differentiate from naive (Tn) to central memory (Tcm), effector memory (Tem), and terminally differentiated effector memory CD45Ra+ (Temra) cells [2]. Regardless of the $\gamma\delta$ TCR subset, the strong cytotoxic properties of $\gamma\delta$ Tem cells play a crucial role in the killing of virus-infected and cancer cells. For decades, TCRV γ 9V δ 2 $\gamma\delta$ T cells have been known to react to cells infected by viruses such as the Epstein–Barr virus (EBV) [3], herpes simplex viruses [4], human immunodeficiency virus (HIV) [5], [6], human papillomavirus (HPV) [7], hepatitis B virus (HBV) [8], Influenza viruses [9,10], dengue virus [11], and severe acute respiratory syndrome-related coronavirus (SARS-CoV) [12]; whereas the TCRV γ non9 lymphocytes [13] respond, inter alia, to cytomegalovirus (CMV), hepatitis E virus (HEV) [14], and Kaposi's sarcoma-associated herpesvirus (HHV-8) [15].

The overall T and $\gamma\delta$ T cell response remain hitherto poorly understood in coronavirus disease 2019 (COVID-19) caused by severe acute respiratory syndrome coronavirus 2 (SARS-CoV-2) infection. Like other respiratory viral infections, COVID-19 can exhibit distinct patterns of clinical features and disease severity, ranging from a virus-induced respiratory pathology due to a weak immune response to an overaggressive immunopathology caused by excessive immune activation. The heterogeneous immune profiles recently characterized in peripheral blood mononuclear cells (PBMC) of COVID-19 patients reflect this wide range of symptoms. COVID-19 patients have a quantitatively decreased compartment of $\gamma\delta$ T cells that are more differentiated than control samples [16], accompanied by an increased number of immature neutrophils [17]. Similar alterations were reported with the other adaptive and unconventional T lymphocytes [18,19], supporting a scenario of broad T cell immunosuppression linked to fatal outcomes [20].

Likewise, the extent and quality of tumor-infiltrating T lymphocytes (TILs) in cancer are important determinants of the outcome of immunotherapy or untreated cancer patients. On the one hand, a weak immune response to cold tumors, peripherally excluding tumors, or tumors infiltrated by exhausted T lymphocytes allows for uncontrolled cancer and leads to fatal outcomes. On the other hand, too strong immune reactions are sometimes observed in untreated cancers (for review [21]) and systematically in patients receiving immune checkpoint blockade. Therefore, viral infections and cancer can present large and heterogeneous spectrums of immune response patterns. In human cancer, our research and other studies have shown that the abundance of $\gamma\delta$ TILs, whether TCRV γ 9 or TCRV γ non9, varies substantially across individuals and among cancer types, and that it is associated with patient outcomes [22,23]. As opposed to peripheral blood and hematopoietic malignancies dominated by TCRV γ 9 $\gamma\delta$ T cells, the predominant subset of $\gamma\delta$ TILs in most solid tumors are TCRV γ non9 cells, whose number, cytotoxic differentiation, and functional status vary between individuals [24–26].

We recently depicted the pan-cancer landscape of human $\gamma\delta$ TILs using single-cell RNA sequencing (scRNAseq). This strategy unveiled that the differentiation of cytotoxic $\gamma\delta$ T cells from the TCRV γ 9 and TCRV γ non9 subsets was related to the CMV status of the healthy donors [27]. Furthermore, despite the considerable heterogeneity of cancer patients, their infiltration and differentiation appeared phased with that of the adaptive T CD8 TIL compartment, yielding correlated rates of functional and/or exhausted $\gamma\delta$ T and T CD8 TILs in human cancers [28].

Overall, these findings raised questions as to whether the viral status of cancer patients affected their $\gamma\delta$ TILs, and whether the transcriptomic profiles correlated with those of T lymphocytes from COVID-19 patients' PBMC. Here, we addressed these questions through a comprehensive characterization of the differentiation and functional hallmarks of $\gamma\delta$ T lymphocytes by analyzing scRNAseq datasets of tumors from cancer patients with known viral status, and PBMC from COVID-19 patients.

2. Materials and Methods

2.1. scRNAseq Datasets Pre-Processing

The (cells, gene) matrix data for the control $\gamma\delta$ T isolated from healthy donor's PBMC has been previously published [28]. The scRNAseq of tumor lesions from Hodgkin's lymphoma (HL) (EGAS00001004085) [29], head and neck squamous cell carcinoma (HNSCC) (GSE139324) [30], PBMC from COVID-19 patients (GSE145926, GSE155224, GSE155249, GSE166489, and GSE167029) were downloaded and assembled to digitally extract their $\gamma\delta$ T lymphocytes. After pre-processing and discarding cell doublets and dying cells, all datasets were integrated using the R package Seurat version 4.0 [31]. Principal components analysis (PCA) was performed on this integrated dataset before uniform manifold approximation and projection (UMAP) [32] to check the integrated dataset quality.

2.2. Single-Cell Signatures and Scores

After normalization and integration, the integrated scRNAseq dataset was scored for a collection of multigene signatures [28] using Single-Cell Signature Explorer software [33]. Briefly, the score of each single-cell C_j for gene set GS_x was computed as the sum of all unique molecular identifiers (UMI) for all the GS_x genes expressed by C_j divided by the sum of all UMI expressed by C_j :

$$\text{Score of cell } C_j \text{ for geneset } GS_x = \left(\sum(\text{UMI})_{GS_x} C_j \right) / \left(\sum(\text{UMI})_{C_j} \right) \quad (1)$$

All cell signature scores were merged with each cell's trajectory coordinates using Single-Cell Signature Merger software [33]. For visualization, Single-Cell Multilayer Viewer was used, a serverless software allowing to merge up to five layers of quantitative and qualitative variables, alone or in combination [28].

2.3. Score and Gate for Digital Extraction of $\gamma\delta$ T Lymphocytes

Starting from any scRNAseq datasets pre-processed as above, this procedure comprised five gating steps sequentially applied using Single-Cell Virtual Cytometer software [34]:

1. Positive selection of double negative cells (= T and NK lineages) from the scatterplot of 'B cell' and 'Myeloid cell' signature scores.
2. Scatterplot of 'B cell' signature against the addition of 'CD8AB' and 'TCR $\gamma\delta$ ' signatures to positively select the double-positive cells (= non-CD4 T cells).
3. Scatterplot of 'CD8ab' signature against 'TCR α constant gene *TRAC*' signature to digitally extract double-positive cells (= $\alpha\beta$ T CD8 lymphocytes) on the one hand, and negative cells (= $\gamma\delta$ T plus CD4CD8-double negative $\alpha\beta$ T cells) on the other hand.
4. Scatterplot of the addition of 'CD3 complex' and 'TCR α constant gene *TRAC*' signatures against the addition of 'CD3 complex' and 'TCR $\gamma\delta$ ' signatures to extract the 'CD3 complex' and 'TCR $\gamma\delta$ ' double-positive cells (= $\gamma\delta$ T lymphocytes).

The datasets of the finally identified $\gamma\delta$ T cells were digitally extracted from the original scRNAseq dataset and further subtyped and injected on the trajectory (see below).

2.4. Subtyping of the TCRV $\gamma 9$ and TCRV $\gamma non9$ $\gamma\delta$ T Cells

This was performed as previously described [28]. Briefly, $\gamma\delta$ T lymphocytes express either the *TRGC1*-encoded TCRV $\gamma 9$ or the *TRGC2*-encoded TCRV $\gamma non9$ in a mutually exclusive fashion, so the extracted $\gamma\delta$ T lymphocytes were categorized as TCRV $\gamma 9$ cells based on ('*TRDC*, *TRGC1*' positive cells) or TCRV $\gamma non9$ cells based on ('*TRDC*, *TRGC2*' positive cells) classifications using a compensated score of these two signatures. Compensated scores were obtained by multiplying the score of the gene set of interest, here $GSS_{TCRV\gamma 9}$, by its difference to its complementary gene set ($GSS_{TCRV\gamma 9}$ minus $GSS_{TCRV\gamma non9}$):

$$GSS_{TCRV\gamma 9 comp} = GSS_{TCRV\gamma 9} \times (GSS_{TCRV\gamma 9} - GSS_{TCRV\gamma non9}) \quad (2)$$

Scatterplots of $GSS_{TCRV\gamma9}$ and $GSS_{TCRV\gamma non9}$ finally identified the TCRV $\gamma9$ or TCRV $\gamma non9$ subset of each $\gamma\delta$ T lymphocyte [28].

2.5. Cells Injection on Public Pseudotimed Differentiation Trajectory

The maturation trajectory of $\gamma\delta$ T cells was computed by minimum spanning tree and visualized as pseudotimed trajectories. Pseudotimed trajectories are differentiation trajectories shown with cell pseudotime on the x -axis and a projection of both trajectory dimensions (here MST1 and MST2) on the y -axis [28]. We will refer below to them as ‘public $\gamma\delta$ T lymphocytes trajectory’ the pseudotimed differentiation trajectory of all $\gamma\delta$ T lymphocytes from ~150 tissues samples, including healthy donors’ PBMC and cancer patients’ tumors (the (cell, gene) matrix data is available from [28]). New $\gamma\delta$ T lymphocytes digitally extracted from additional datasets, such as those from COVID-19 patients, were injected onto this ‘public $\gamma\delta$ T cell trajectory’. Briefly, a total of ($n = 9$) datasets for COVID-19-derived tissues were downloaded. These COVID-19 datasets were first filtered for quality control, integrated as described above, and their $\gamma\delta$ T lymphocytes were digitally extracted by score and gate [28]. These new $\gamma\delta$ T lymphocytes were then injected onto the public trajectory by using Seurat’s Integration and Map-to-Query workflow to determine their respective (MST1, MST2) coordinates and then infer their pseudotime within the public trajectory. This procedure encompasses the following four steps:

Step 1:

- Query 1 = $\gamma\delta$ T lymphocytes digitally extracted from COVID-19 samples;
- Reference = public trajectory;
- Integration of gene expression data from Query 1 and Reference (Seurat’s Integration).

Step 2:

- Query 2 = Integrated (Query and Reference);
- Reference = public trajectory;
- Transferring MST coordinates from Reference metadata to Query 2 (Seurat’s Map-to-Query).

Step 3:

- Query 2 = pseudotime calculation using MST coordinates and R package Dynverse.

Step 4:

- Visualization of new data (Query 1) on the public trajectory (Reference) using Single-Cell Multilayer Viewer [28].

2.6. Classifications

The TILs classifications as Ttrm/non-Ttrm and Tex/non-Tex were performed by ‘at least one binary’. Briefly, the single cells were scored for several reference gene signatures as previously described [28]. For Tex classification, the reference Tex signatures were based on five published and partially overlapping Tex gene sets [35–39]. For each signature, a cut-off was defined as the maximal score of the ($n = 3680$) control $\gamma\delta$ T lymphocytes extracted PBMC of healthy adults. This threshold defined the cell’s binary (1: cell score > threshold, 0: otherwise). The Tex cut-offs were: 3.9 for ‘Chihara_IL27_Coinhib_module’ [35]; 0.52 for ‘Alfei_d20_tox’ [36]; 0.22 for ‘Khan_ToX_OverExpressed_genes’ [37]; 0.5 for ‘Tosolini_NHL_IEGS33’ [38]; and 0.16 for ‘Balanca_QP_genes’ [39]. For each TIL, the five Tex binaries were summed, and if the sum was non-zero, the TIL was classified as Tex, or otherwise as non-Tex. The Ttrm classification was applied likewise using six references and partially overlapping Ttrm signatures published previously [40,41]. The binarizing cutoffs established with the control $\gamma\delta$ T lymphocytes were: 0.46 for ‘Kumar_13g_Ttrm’; 0.3 for ‘Kumar_3g_Ttrm’ [40]; 3.72 for ‘Wu_Tcellcluster4.1_trm’; 2.6 for ‘Wu_Tcellcluster8.3_trm’; 2.8 for ‘Wu_Tcellcluster8.3b_trm’; 4.2 for ‘Wu_Tcellcluster8.3c_trm’ [41]. These Ttrm binaries were summed, and if the sum was non-zero, the TIL was classified as Ttrm, or otherwise as non-Ttrm (recirculating).

3. Results

3.1. Tumor Infiltrating $\gamma\delta$ T Lymphocytes from Virus-Positive and -Negative Cancer Patients

We downloaded the published scRNAseq dataset from a total of ($n = 26$) human tumors of head and neck carcinoma (HNSCC), including ($n = 8$) samples positive and ($n = 18$) negative for HPV, as well as ($n = 9$) Hodgkin's lymphoma (HL) of mixed cellularity subtype in which ($n = 5$) samples were positive and ($n = 4$) negative for EBV. Their respective $\gamma\delta$ T lymphocytes were digitally purified, and their TCR subtype and differentiation stage were determined by injection onto the 'public $\gamma\delta$ T cell trajectory' (see Methods) and cross-labeling with reference gene signatures from external single-cell datasets of human TILs [28].

A total of ($n = 1055$) $\gamma\delta$ TILs (($n = 401$) TCRV γ 9 plus ($n = 654$) TCRV γ non9 cells) were extracted from HNSCC, and ($n = 113$) $\gamma\delta$ TILs (($n = 51$) TCRV γ 9 plus ($n = 62$) TCRV γ non9 cells) from HL. In contrast with PBMC from healthy donors, the cell counts extracted from tumors varied considerably across individuals and in both diseases (range: 1–33 $\gamma\delta$ TILs in HL patients, and 0–111 in HNSCC patients), as previously reported in other cancer types [28]. On average, HNSCC comprised more $\gamma\delta$ TILs (mean = 40 cells, 15 TCRV γ 9 + 25 TCRV γ non9) than HL (mean = 13 cells, 6 TCRV γ 9 + 7 TCRV γ non9; t -test $P = 3 \times 10^{-4}$). The rates of their Tn, Tcm, Tem, and Temra stages varied between patients but without reaching significant difference between cancers and viral status (mean in HNSCC: 15% Tn, 37% Tcm, 47% Tem, 0.9% Temra; mean in HL: 9% Tn, 35% Tcm, 55% Tem, 0.8% Temra) (Figure 1a). In both cancers, these recirculating (non-Ttrm TILs, Methods) $\gamma\delta$ TILs comprised less exhausted cells than their tissue-resident (Ttrm) counterparts (15% and 37%, respectively). Furthermore, the rates of recirculating $\gamma\delta$ TILs were significantly associated with patient's viral status (χ^2 P value = 7.8×10^{-18}): tumors of viral-positive HL and HNSCC included far more recirculating $\gamma\delta$ TILs than viral-negative tumors (80% vs. 45% of $\gamma\delta$ TILs, respectively) (Figure 1b).

Altogether, these data demonstrate that patients with HPV-positive HNSCC and EBV-positive HL have $\gamma\delta$ TILs more prone to recirculate from the tumor and avoid exhaustion.

3.2. $\gamma\delta$ T Lymphocytes from COVID-19 Patients

The scRNAseq datasets from PBMC of ($n = 43$) COVID-19 patients and ($n = 21$) healthy controls, as well as from broncho-alveolar lavage fluids (BALF) from ($n = 20$) COVID-19 patients and ($n = 4$) healthy controls were downloaded. A total of ($n = 7473$) $\gamma\delta$ T lymphocytes were digitally extracted from these datasets, and their TCR subtype and differentiation stage were characterized as described above (see Methods).

In spite of similar dataset sizes, each sample of COVID-19 PBMC yielded on average three times less $\gamma\delta$ T lymphocytes than the healthy controls (100 vs. 330, respectively, t -test $P = 4 \times 10^{-5}$), and both TCR subsets had decreased cell counts (on average 63 vs. 142 TCRV γ 9 and 37 vs. 187 TCRV γ non9 in COVID-19 vs. control samples, respectively). Parallel analyses showed on average $n = 561$ and $n = 479$ T CD8 cells per sample in the same groups indicating that the COVID-19-related lympho-reduction from PBMC is specific to the $\gamma\delta$ T cell lineage (Chi-2 P value = 5×10^{-27}).

However, their differentiation stages remained unchanged between healthy and COVID-19 PBMC (7% Tn, 25% Tcm, 66% Tem, 3% Temra among TCRV γ 9 cells; 19% Tn, 30% Tcm, 50% Tem, 2% Temra among TCRV γ non9 cell) (Figure 2a,b). In contrast, BALF of COVID-19 patients encompassed more $\gamma\delta$ T lymphocytes than control BALF (on average 16 vs. 0 $\gamma\delta$ T per BALF, respectively). Such COVID-19 BALF-derived $\gamma\delta$ T encompassed both subsets (on average nine TCRV γ 9 and seven TCRV γ non9 cells) and were more differentiated than in PBMC (on average 1% Tn, 18% Tcm, 81% Tem, 0% Temra among TCRV γ 9 cells; 3% Tn, 36% Tcm, 61% Tem, 0% Temra among TCRV γ non9). Furthermore, the Ttrm gene signature was expressed by scarce (0.3%) $\gamma\delta$ T lymphocytes in the control PBMC, but by 4% in COVID-19 PBMC and 17% in the COVID-19 BALF. Likewise, the Tex signature was up-regulated by 0%, 1%, and 24% $\gamma\delta$ T lymphocytes, respectively, from these COVID-19 BALF samples (Figure 2a,b).

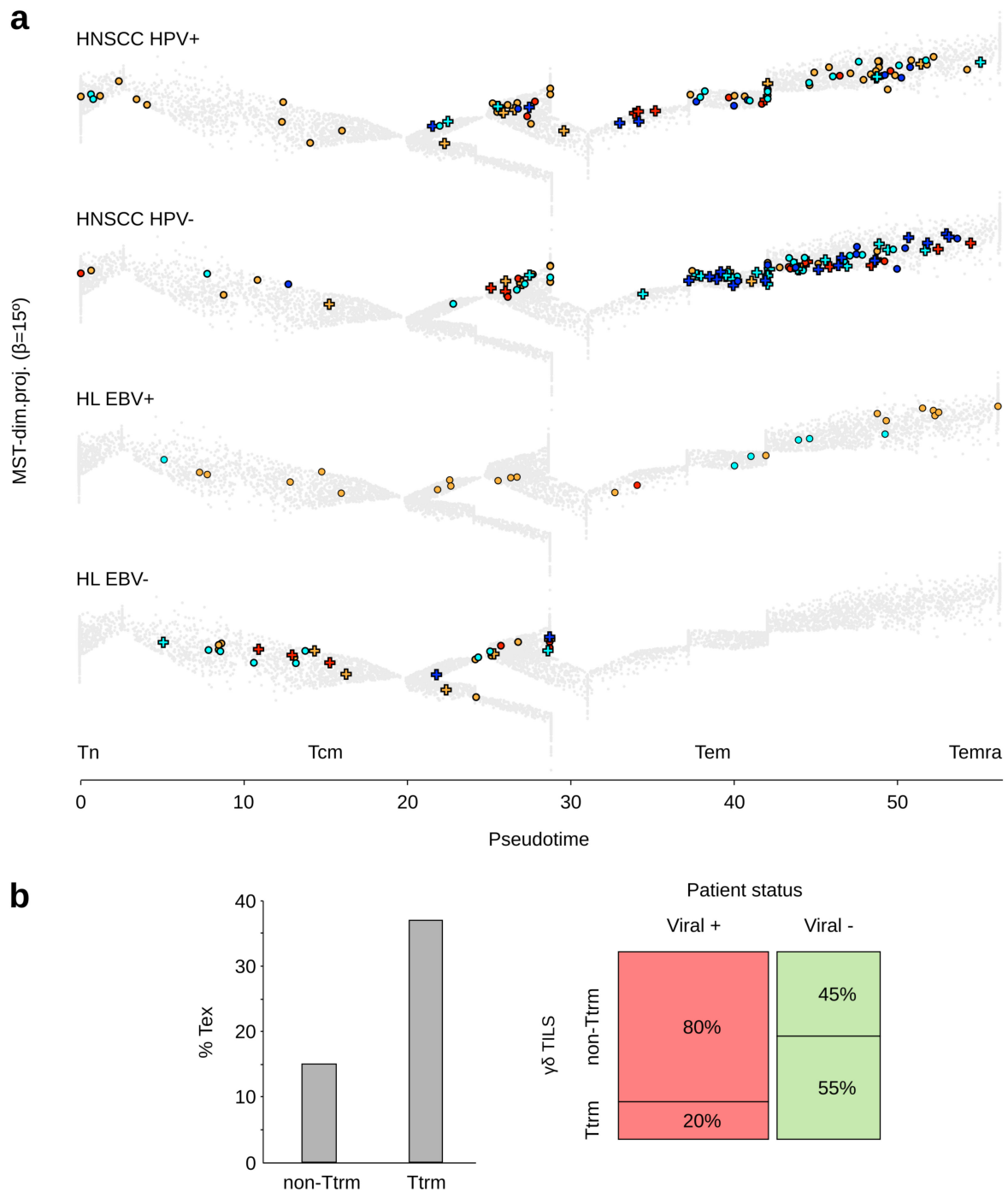


Figure 1. Differentiation and functional hallmarks of $\gamma\delta$ T lymphocytes infiltrating HNSCC and HL tumors according to viral status of cancer patients. (a) Examples of $\gamma\delta$ TILs extracted from representative HNSCC and HL tumors with viral status, overlaid on the public trajectory of $\gamma\delta$ T lymphocytes reference (grey). Key: TCRV γ 9 cells (light blue), Tex TCRV γ 9 cells (dark blue), TCRV γ non9 cells (orange), Tex TCRV γ non9 cells (dark red), recirculating (non-Ttrm) cells (open circles), Ttrm (cross). Differentiation pseudotime scale: 0–5: Tn, 5–20: Tcm, 20–50: Tem; > 50: Temra. Together all the EBV-negative HL tumors totaled 53 mostly functional (43/53, 81%) $\gamma\delta$ TILs, including 13 Ttrm with 39% of exhausted cells (5/13 Ttrm), while all the EBV-positive HL tumors totaled 60 mostly functional (56/60, 93%) $\gamma\delta$ TILs, including 2 non-exhausted Ttrm $\gamma\delta$ TILs. The HPV-negative HNSCC tumors totaled 698 mostly functional (489/698, 70%) $\gamma\delta$ TILs, including 326 Ttrm with 39% of exhausted cells (127/326 Ttrm), while the HPV-positive HNSCC tumors totaled 357 mostly functional (310/357, 87%) $\gamma\delta$ TILs, including 81 Ttrm with 31% of exhausted cells (25/81 Ttrm). (b) Right: rates of recirculating and Ttrm among $\gamma\delta$ TILs (both subsets) per viral status of patients (pooled); left: rates of exhausted cells among the recirculating and Ttrm $\gamma\delta$ TILs.

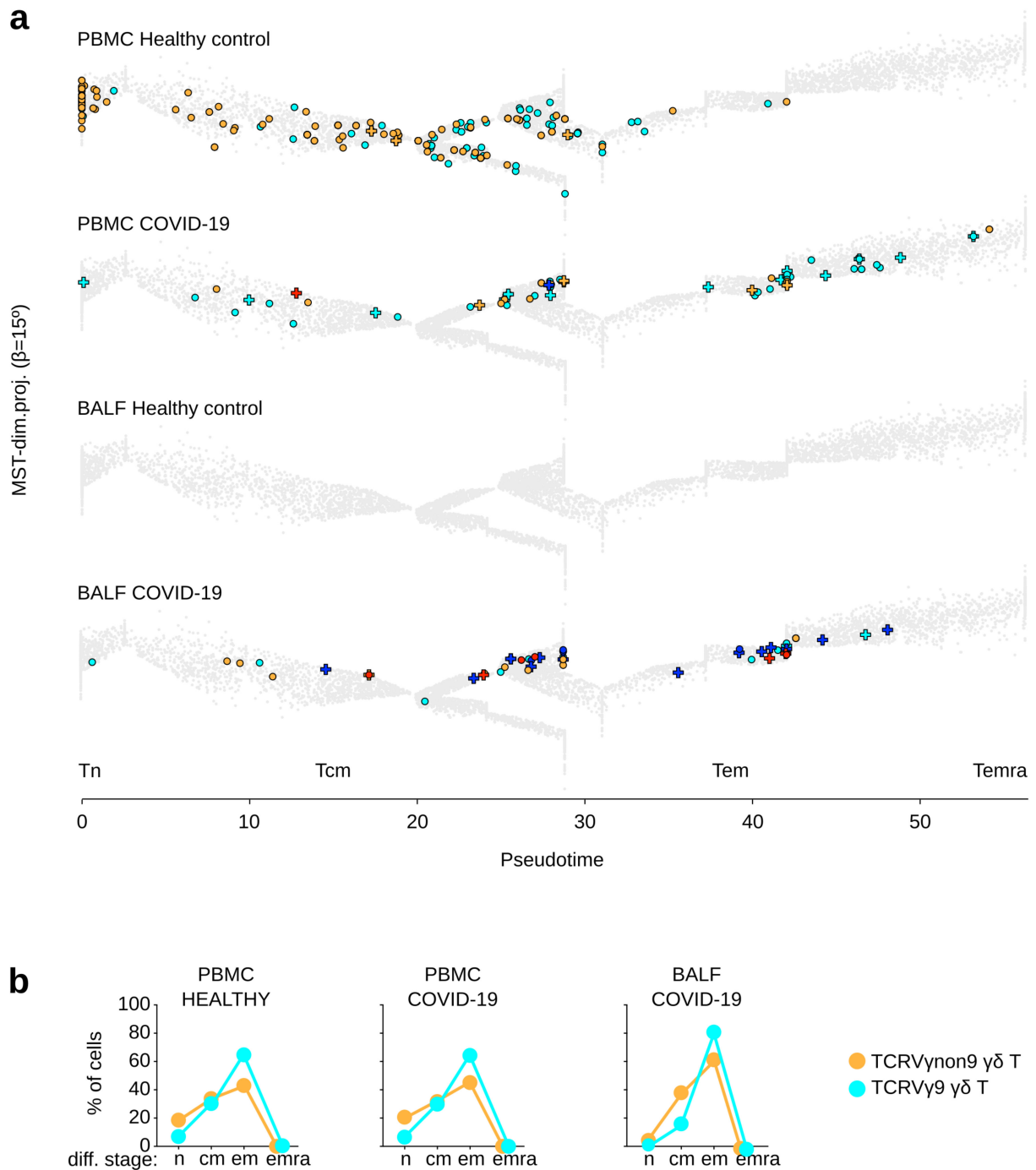


Figure 2. Differentiation and functional hallmarks of $\gamma\delta$ T lymphocytes from control donor’s PBMC and BALF. (a) $\gamma\delta$ T lymphocytes extracted from PBMC and BALF of healthy individuals and COVID-19 patients. No $\gamma\delta$ T lymphocyte was found in any of the healthy control’s BALF (representative examples, cells are shown overlaid on the public trajectory of $\gamma\delta$ T lymphocyte differentiation, same legend key as in Figure 1). (b) Rates of cells at each differentiation stage among the TCRV γ 9 and TCRV γ non9 $\gamma\delta$ T lymphocytes (group means are shown).

These data suggest that in adult COVID-19 patients, both subsets of $\gamma\delta$ T lymphocytes relocate from PBMC to the infected lung tissue, where their advanced differentiation, tissue residency, and exhaustion hallmarks witness of a recent T cell activation.

3.3. $\gamma\delta$ T Lymphocytes in Clinical Groups of Adult Patients with COVID-19

These $\gamma\delta$ T cell analyses were then extended to clinical subgroups of adult COVID-19 patients. The total number of $\gamma\delta$ T lymphocytes in BALF of adult COVID-19 patients varied considerably between individuals without reaching a statistical difference between mild ($n = 2$) and severe ($n = 6$) disease (on average 39 vs. 22 $\gamma\delta$ T cells per sample, respectively). The TCRV γ 9 cell counts were similar in both groups (on average 13 vs. 14 cells per sample, respectively), whereas the TCRV γ non9 cell counts decreased in severe COVID-19 (on average 26 vs. 7) despite maintaining the same differentiation stage pattern (on average 1% Tn, 37% Tcm, 62% Tem, 0% Temra). Of note, with 0% Tn, 20% Tcm, 80% Tem, and 0% Temra in both groups, the TCRV γ 9 cells were more differentiated than the TCRV γ non9 cells. The $\gamma\delta$ T lymphocytes in BALF of patients with mild disease included 9% Ttrm and 12% Tex cells, contrasting to 40% Ttrm and 40% Tex in severe disease, and both subsets behaved similarly (Figure 3a). Hence, acute COVID-19 increases both tissue residency and exhaustion of $\gamma\delta$ T lymphocytes in infected lung lesions.

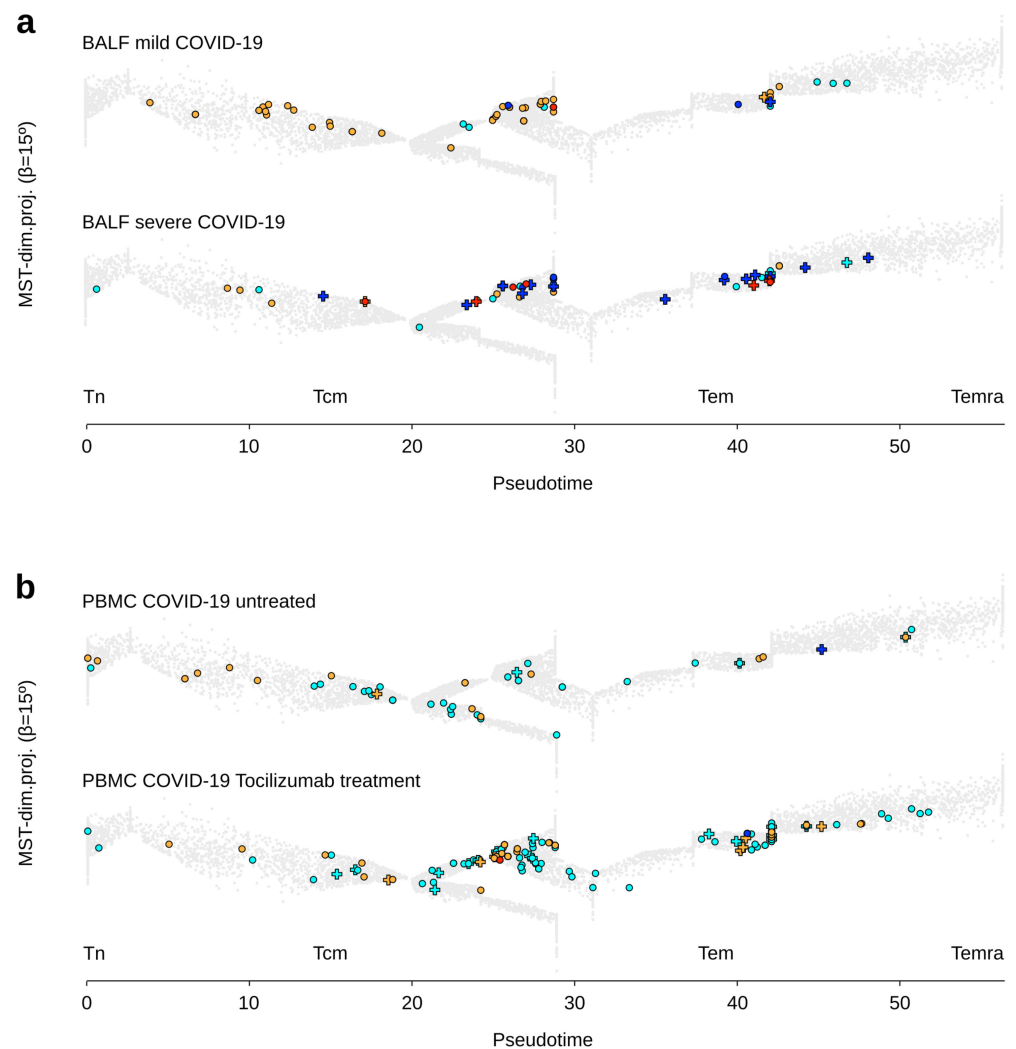


Figure 3. Differentiation and functional hallmarks of $\gamma\delta$ T lymphocytes from adult COVID-19 patients. (a) BALF-derived $\gamma\delta$ T lymphocytes from adult patients with mild or severe COVID-19 disease. (b) PBMC-derived $\gamma\delta$ T lymphocytes from adult COVID-19 patients untreated or treated with Tocilizumab. (Representative examples overlaid on the public trajectory of $\gamma\delta$ T lymphocyte differentiation, same legend key as in Figure 1).

The PBMC of adult COVID-19 patients treated ($n = 12$) or not ($n = 4$) by Tocilizumab, an anti-IL-6R mAb drug, had similar cell counts of total $\gamma\delta$ T lymphocytes (on average 59 vs. 45 $\gamma\delta$ T cells per sample, respectively), as for both TCRV γ 9 and TCRV γ non9 subsets. Meanwhile, Tocilizumab clearly promoted both subsets' differentiation (TCRV γ 9 untreated: 8% Tn, 29% Tcm, 61% Tem, 2% Temra; TCRV γ 9 treated: 2% Tn, 11% Tcm, 85% Tem, 2% Temra; TCRV γ non9 untreated: 30% Tn, 31% Tcm, 39% Tem, 0% Temra; both subsets treated: 9% Tn, 16% Tcm, 74% Tem, 1% Temra). This treatment did not affect their low rates of Tex cells (Figure 3b). Therefore, anti-IL6R treatment favors $\gamma\delta$ T lymphocyte differentiation in COVID-19 patients.

3.4. $\gamma\delta$ T Lymphocytes in Clinical Groups of Pediatric Patients with COVID-19

Finally, we analyzed the $\gamma\delta$ T cell landscape in PBMC of children with acute COVID-19 ($n = 5$), multisystem inflammatory syndrome (MIS-C) ($n = 14$), and healthy pediatric controls ($n = 7$). The PBMC of pediatric controls comprised more $\gamma\delta$ T lymphocytes of both TCR subsets than the PBMC of adult controls ($n = 4$) (average $\gamma\delta$ T cell counts: 393 vs. 220, respectively), although their differentiation was similar (TCRV γ 9: 5% Tn, 43% Tcm, 51% Tem, 2% Temra; TCRV γ non9: 14% Tn, 45% Tcm, 40% Tem, 1% Temra) (Figure 4a).

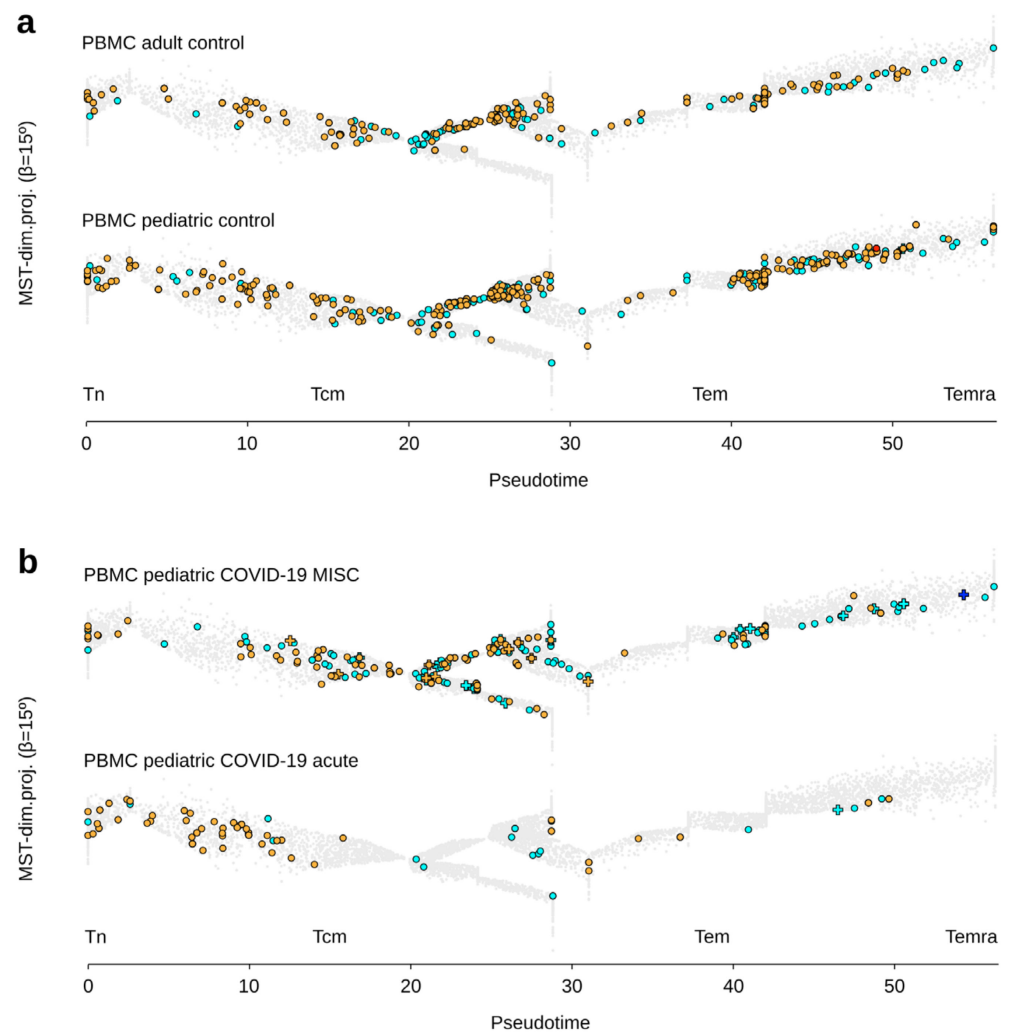


Figure 4. Differentiation and functional hallmarks of $\gamma\delta$ T lymphocytes from pediatric COVID-19 patients. (a) PBMC-derived $\gamma\delta$ T lymphocytes from adult and pediatric controls. (b) PBMC-derived $\gamma\delta$ T lymphocytes from pediatric COVID-19 patients with either MIS-C or acute disease. (Representative examples overlaid on the public trajectory of $\gamma\delta$ T lymphocyte differentiation, same legend key as in Figure 1).

PBMC from acute and MIS-C COVID-19 children comprised less $\gamma\delta$ T lymphocytes of both subsets than the pediatric controls (average $\gamma\delta$ T cell counts: 71 (acute), 163 (MIS-C) vs. 393 (controls)). They were also less differentiated in acute disease than in MIS-C and pediatric controls (acute: TCRV γ 9: 14% Tn, 52% Tcm, 34% Tem, 0% Temra; TCRV γ non9: 37% Tn, 44% Tcm, 19% Tem, 0% Temra; MIS-C: TCRV γ 9: 10% Tn, 26% Tcm, 61% Tem, 3% Temra; TCRV γ non9: 22% Tn, 28% Tcm, 50% Tem, 1% Temra). Last but not least, the PBMC of pediatric controls contained no Tex cell among $\gamma\delta$ T lymphocytes (in both subsets), as in the acute COVID-19 samples, but $n = 2$ Tex out of 2285 cells were detected in MIS-C samples (Figure 4b).

Together, these results indicated that acute COVID-19 disease induces a similar $\gamma\delta$ T cell lymphopenia PBMC of pediatric and adult patients. In contrast, the PBMC-derived $\gamma\delta$ T cells from MIS-C patients with SARS-CoV-2 infection are not lymphodepleted and resemble to those from healthy PBMC.

4. Discussion

In single-cell transcriptomics, pseudotime describes the progression of each cell alongside a continuous series of differentiation states, through a non-linear transformation of real chronological time [42–44]. How explicit time is quantitatively converted into $\gamma\delta$ T cell pseudotime remains to be determined, and depends on the transcriptome diversity and the total number of single cells in the dataset. All the features of differentiation trajectories are strictly dependent upon the number of single cells selected. Hence, once a trajectory has been inferred from a given single-cell dataset, adding *ab extra* single cells to this dataset will change the trajectory, preventing their mapping on the former map. Here, we addressed this issue by incepting a method to inject without distortion any amount of *ab extra* cells on the reference trajectory.

In this way, we were able to map and thus characterize thousands of $\gamma\delta$ T lymphocytes from newer datasets onto a formerly-built reference map called here ‘public $\gamma\delta$ T cell trajectory’ [28]. Of note, this trajectory encompasses a remarkable set of $\gamma\delta$ T lymphocytes, being currently paved with ~30,000 $\gamma\delta$ T cells from ~220 healthy and diseased adult individuals. As a result, it achieves a much higher level of exhaustivity and resolution than is possible with the cells from a single individual alone. Together, the public $\gamma\delta$ T cell trajectory and the method for mapping newer $\gamma\delta$ T cells provide a unique resource for characterizing these lymphocytes from diverse sources at the highest level of resolution.

As a result of high-resolution mapping of thousands of $\gamma\delta$ T lymphocytes from patients with cancer or COVID-19, we were able to gain a wealth of information about $\gamma\delta$ T lymphocyte differentiation dynamics at the single-cell scale. As reviewed in this series, the role of human $\gamma\delta$ T cells in viral infections is highly investigated and debated in the context of SARS-CoV-2 infection [45–48]. Here, we found in PBMC of COVID-19 patients that $\gamma\delta$ T lymphocytes were decreased compared to control samples, a finding consistent with flow cytometry studies [16,20,49,50]. Although a peripheral lymphopenia in COVID-19 was initially thought to indicate T cell immunosuppression, our present maps and other studies [18] show that $\gamma\delta$ T cells increase concurrently in BALF of COVID-19 patients. T cell exhaustion is rarely observed among the $\gamma\delta$ T cells in PBMC from adult and pediatric patients with COVID-19, even during its acute phase as reported with HEV infection [14]. Most Tex $\gamma\delta$ T cells were instead found in the infected lung rather than in the circulating blood. Hence, COVID-19-induced $\gamma\delta$ T cell exhaustion likely represents a scar of recent localized T cell activation in both TCRV γ 9 and TCRV γ non9 subsets of cells rather than in a single subset alone [17]. Moreover, their advanced differentiation stages in blood from children with multisystem inflammatory syndrome associated with SARS-CoV-2 infection further support this view [51]. Tocilizumab, an IL-6 pathway inhibitor, effectively reduces mortality of severely ill and lymphopenic COVID-19 patients, notably by attenuating inflammation and normalizing their circulating T cell rates [52,53]. Consistent with these reports, the increased effector memory cells we observed here indicates that Tocilizumab

also promotes $\gamma\delta$ T cell differentiation, which constitutes a bioactivity of dual interest for both antiviral [45] and anticancer [54] immunity.

Single-cell studies have shown that the differentiation dynamics of human $\gamma\delta$ T lymphocytes in both TCRV γ 9 and TCRV γ non9 subsets primarily reflect the transcriptional emergence of their cytotoxic function, which peaks at the Tem and Temra stages [27]. In many solid and hematological human cancers, both lineages of $\gamma\delta$ T and T CD8 TILs present strikingly coherent differentiation profiles, and a sizeable fraction of $\gamma\delta$ T TILs are tissue-resident memory and exhausted cells [28]. Many T CD8 TILs in melanoma are bystander cytotoxic lymphocytes with a TCR specificity for viral antigens (V-spe), while only a minority represent true tumor-antigen-specific (T-spe) lymphocytes [55]. Among such CD8 TILs, the V-spe clonotypes prominently display functional Tcm and Tem differentiation stages whereas the majority of T-spe clonotypes are dysfunctional Tex cells [56]. In parallel, we found that HPV-positive HNSCC and EBV-positive HL patients have $\gamma\delta$ TILs that are more prone to recirculate from the tumor and avoid exhaustion. Considering the above findings, it is tempting to hypothesize that a contingent of peripheral $\gamma\delta$ T lymphocytes induced by viral infections does persist in the long term in the blood of adult individuals as central/effector memory cells, and can readily infiltrate tumors to mediate a large spectrum of HLA-unrestricted cytotoxic activities despite true antigen specificity.

For its clinical relevance to cancer immunotherapy, future studies from our team will seek to discern at the single-cell level the T-spe and V-spe clonotypes persisting among the human $\gamma\delta$ T lymphocytes in the peripheral blood and infiltrating tumors. Further, our study provides a fundamental framework for characterizing $\gamma\delta$ T lymphocytes in viral diseases and cancers, and provides the community with a unique resource for the monitoring of human $\gamma\delta$ T lymphocytes at high-resolution.

Author Contributions: J.-J.F. and J.P.C. conceived and designed the study; J.P.C. conceived methods, processed, and performed bioinformatic data analyses; J.-J.F. and J.P.C. generated figures, and wrote the manuscript; M.P., F.P. and M.T. conceived algorithms; C.L., S.B. and J.-J.F. supervised the study; all authors revised the manuscript. All authors have read and agreed to the published version of the manuscript.

Funding: This work was supported by institutional grants from the Institut National de la Santé et de la Recherche Médicale (INSERM), the Université Toulouse 3-Paul Sabatier (UPS), the Centre National de la Recherche Scientifique (CNRS); Laboratoire d'Excellence Toulouse Cancer (TOUCAN-2) under grant contract ANR11-LABX; the Fondation ARC under grant contract PGA1-RF2019-0208691; the Institut Universitaire du Cancer de Toulouse-Oncopole under contract CIEL; the Institut Carnot Lymphome under contract CALYM. This work was granted access to the HPC resources of CALMIP supercomputing center under allocation 2020-T19001.

Institutional Review Board: Not applicable.

Informed Consent Statement: Not applicable, the presented study did not involve novel tissue samples from humans or animals.

Data Availability Statement: Further information and reasonable requests for resources and processed data, such as integrated (cell, UMI) matrices of extracted $\gamma\delta$ T and their corresponding cell annotations, should be directed to J.-J.F. (jean-jacques.fournie@inserm.fr) or J.P.C. (juan-pablo.cerapio-arroyo@inserm.fr). Source scRNAseq datasets used in this study are available at GEO with the accession numbers: GSE139324, GSE145926, GSE155224, GSE155249, GSE166489, and GSE167029; and at the European Genome-Phenome Archive (EGA) with the accession number: EGAS00001004085. Single-Cell Multilayer Viewer (scMLV) is available on GitHub repository: <https://github.com/MarionPerrier/scMLV> (accessed on 31 March 2021). Single-Cell Signature Scorer and Single-Cell Virtual Cytometer are available at: <https://sites.google.com/site/fredsoftwares/products> (accessed on 12 October 2021). Seurat v4 is available from the Comprehensive R Archive Network (CRAN) and further details in the installation can be found on <https://satijalab.org/seurat/> (accessed on 12 October 2021).

Acknowledgments: The authors thank CRCT collaborators for their support and their critical discussions.

Conflicts of Interest: The authors declare no relevant conflict of interest.

Abbreviations

The following abbreviations are used in this manuscript

CMV	cytomegalovirus
COVID-19	coronavirus disease 2019
EBV	Epstein–Barr virus
HEV	hepatitis E virus
HL	Hodgkin’s lymphoma
HNSCC	head and neck squamous cell carcinoma
HPV	human papillomavirus
MIS-C	multisystem inflammatory syndrome in children
PBMC	peripheral blood mononuclear cells
SARS-CoV	severe acute respiratory syndrome-related coronavirus
scRNAseq	single-cell RNA sequencing
Tcm	central memory T
Tem	effector memory T
Temra	effector memory CD45RA T
Tex	exhausted T
TIL	tumor-infiltrated lymphocyte
Tn	naive T
Ttrm	tissue-resident memory T

References

- Hayday, A.C.; Vantourout, P. The Innate Biologies of Adaptive Antigen Receptors. *Annu. Rev. Immunol.* **2020**, *38*, 487–510. [[CrossRef](#)] [[PubMed](#)]
- Dieli, F.; Poccia, F.; Lipp, M.; Sireci, G.; Caccamo, N.R.; DI Sano, C.; Salerno, A. Differentiation of Effector/Memory V δ 2 T Cells and Migratory Routes in Lymph Nodes or Inflammatory Sites. *J. Exp. Med.* **2003**, *198*, 391–397. [[CrossRef](#)] [[PubMed](#)]
- Sturm, E.; Braakman, E.; Fisch, P.; Vreugdenhil, R.J.; Sondel, P.; Bolhuis, R.L. Human V Gamma 9-V Delta 2 T Cell Receptor-Gamma Delta Lymphocytes Show Specificity to Daudi Burkitt’s Lymphoma Cells. *J. Immunol.* **1990**, *145*, 3202–3208. [[PubMed](#)]
- Sciammas, R.; Johnson, R.M.; I Sperling, A.; Brady, W.; Linsley, P.S.; Spear, P.G.; Fitch, F.W.; Bluestone, J. Unique Antigen Recognition by a Herpesvirus-Specific Tcr-Gamma Delta Cell. *J. Immunol.* **1994**, *152*, 5392–5397.
- Wallace, M.; Scharko, A.M.; Pauza, C.D.; Fisch, P.; Imaoka, K.; Kawabata, S.; Fujihashi, K.; Kiyono, H.; Tanaka, Y.; Bloom, B.R.; et al. Functional gamma delta T-lymphocyte defect associated with human immunodeficiency virus infections. *Molecular Med. Eng.* **1997**, *3*, 60–71. [[CrossRef](#)]
- Poccia, F.; Gougeon, M.-; Agrati, C.; Montesano, C.; Martini, F.; Pauza, C.; Fisch, P.; Wallace, M.; Malkovsky, M. Innate T-Cell Immunity in HIV Infections: The Role of Vg9Vd2 T Lymphocytes. *Curr. Mol. Med.* **2002**, *2*, 769–781. [[CrossRef](#)]
- Hong, K.; Greer, C.; Ketter, N.; Van Nest, G.; Paliard, X. Isolation and characterization of human papillomavirus type 6-specific T cells infiltrating genital warts. *J. Virol.* **1997**, *71*, 6427–6432. [[CrossRef](#)]
- Ozaki, S.; Ogasahara, K.; Kosaka, M.; Inoshita, T.; Wakatsuki, S.; Uehara, H.; Matsumoto, T. Hepatosplenic gamma delta T-cell lymphoma associated with hepatitis B virus infection. *J. Med. Investig.* **1998**, *44*, 215–217.
- Qin, G.; Mao, H.; Zheng, J.; Sia, S.F.; Liu, Y.; Chan, P.L.; Lam, K.; Peiris, J.S.M.; Lau, Y.; Tu, W. Phosphoantigen-Expanded Human $\gamma\delta$ T Cells Display Potent Cytotoxicity against Monocyte-Derived Macrophages Infected with Human and Avian Influenza Viruses. *J. Infect. Dis.* **2009**, *200*, 858–865. [[CrossRef](#)]
- Sant, S.; Jenkins, M.R.; Dash, P.; Watson, K.; Wang, Z.; Pizzolla, A.; Koutsakos, M.; Nguyen, T.H.; Lappas, M.; Crowe, J.; et al. Human $\gamma\delta$ T-cell receptor repertoire is shaped by influenza viruses, age and tissue compartmentalisation. *Clin. Transl. Immunol.* **2019**, *8*, e1079. [[CrossRef](#)]
- Tsai, C.-Y.; Liang, K.H.; Gunalan, M.G.; Liang, L.D.S.; Lim, D.S.L.; Fisher, D.A.; Macary, P.A.; Leo, Y.S.; Wong, S.-C.; Puan, K.J.; et al. Type I IFNs and IL-18 Regulate the Antiviral Response of Primary Human $\gamma\delta$ T Cells against Dendritic Cells Infected with Dengue Virus. *J. Immunol.* **2015**, *194*, 3890–3900. [[CrossRef](#)]
- Poccia, F.; Agrati, C.; Castilletti, C.; Bordi, L.; Gioia, C.; Horejsh, D.; Ippolito, G.; Chan, P.; Hui, D.; Sung, J.J.Y.; et al. Anti-Severe Acute Respiratory Syndrome Coronavirus Immune Responses: The Role Played by V γ 9V δ 2 T Cells. *J. Infect. Dis.* **2006**, *193*, 1244–1249. [[CrossRef](#)]
- Déchanet, J.; Merville, P.; Lim, A.; Retière, C.; Pitard, V.; Lafarge, X.; Michelson, S.; Méric, C.; Hallet, M.-M.; Kourilsky, P.; et al. Implication of $\gamma\delta$ T cells in the human immune response to cytomegalovirus. *J. Clin. Investig.* **1999**, *103*, 1437–1449. [[CrossRef](#)]
- Barragué, H.; Fontaine, J.; Abravanel, F.; Mauré, E.; Péron, J.-M.; Alric, L.; Dubois, M.; Izopet, J.; Champagne, E. Mobilization of $\gamma\delta$ T Cells and IL-10 Production at the Acute Phase of Hepatitis E Virus Infection in Cytomegalovirus Carriers. *J. Immunol.* **2021**, *206*, 1027–1038. [[CrossRef](#)]
- Barcy, S.; De Rosa, S.C.; Vieira, J.; Diem, K.; Ikoma, M.; Casper, C.; Corey, L. $\gamma\delta$ +T Cells Involvement in Viral Immune Control of Chronic Human Herpesvirus 8 Infection. *J. Immunol.* **2008**, *180*, 3417–3425. [[CrossRef](#)]

16. Rijkers, G.; Vervenne, T.; Van Der Pol, P. More bricks in the wall against SARS-CoV-2 infection: Involvement of $\gamma\delta 2$ T cells. *Cell. Mol. Immunol.* **2020**, *17*, 771–772. [[CrossRef](#)]
17. Carissimo, G.; Xu, W.; Kwok, I.; Abdad, M.Y.; Chan, Y.-H.; Fong, S.-W.; Puan, K.J.; Lee, C.Y.-P.; Yeo, N.K.-W.; Amrun, S.N.; et al. Whole blood immunophenotyping uncovers immature neutrophil-to-VD2 T-cell ratio as an early marker for severe COVID-19. *Nat. Commun.* **2020**, *11*, 1–12. [[CrossRef](#)]
18. Jouan, Y.; Guillon, A.; Gonzalez, L.; Perez, Y.; Boisseau, C.; Ehrmann, S.; Ferreira, M.; Daix, T.; Jeannet, R.; François, B.; et al. Phenotypical and functional alteration of unconventional T cells in severe COVID-19 patients. *J. Exp. Med.* **2020**, *217*. [[CrossRef](#)]
19. Li, C.-X.; Chen, J.; Lv, S.-K.; Li, J.-H.; Li, L.-L.; Hu, X. Whole-Transcriptome RNA Sequencing Reveals Significant Differentially Expressed mRNAs, miRNAs, and lncRNAs and Related Regulating Biological Pathways in the Peripheral Blood of COVID-19 Patients. *Mediat. Inflamm.* **2021**, *2021*, 1–22. [[CrossRef](#)]
20. Kalicińska, E.; Szymczak, D.; Zińczuk, A.; Adamik, B.; Smiechowicz, J.; Skalec, T.; Nowicka-Suszko, D.; Biernat, M.; Bogucka-Fedorczuk, A.; Rybka, J.; et al. Immunosuppression as a Hallmark of Critical COVID-19: Prospective Study. *Cells* **2021**, *10*, 1293. [[CrossRef](#)]
21. Shah, A.A.; Casciola-Rosen, L.; Rosen, A. Review: Cancer-Induced Autoimmunity in the Rheumatic Diseases. *Arthritis Rheumatol.* **2015**, *67*, 317–326. [[CrossRef](#)]
22. Meraviglia, S.; Presti, E.L.; Tosolini, M.; La Mendola, C.; Orlando, V.; Todaro, M.; Catalano, V.; Stassi, G.; Cicero, G.; Vieni, S.; et al. Distinctive features of tumor-infiltrating $\gamma\delta$ T lymphocytes in human colorectal cancer. *OncolImmunology* **2017**, *6*, e1347742. [[CrossRef](#)]
23. Gentles, A.J.; Newman, A.; Liu, C.L.; Bratman, S.; Feng, W.; Kim, D.; Nair, V.S.; Xu, Y.; Khuong, A.; Hoang, C.D.; et al. The prognostic landscape of genes and infiltrating immune cells across human cancers. *Nat. Med.* **2015**, *21*, 938–945. [[CrossRef](#)]
24. Wu, Y.; Kyle-Cezar, F.; Woolf, R.T.; Naceur-Lombardelli, C.; Owen, J.; Biswas, D.; Lorenc, A.; Vantourout, P.; Gazinska, P.; Grigoriadis, A.; et al. An innate-like $V\delta 1 + \gamma\delta$ T cell compartment in the human breast is associated with remission in triple-negative breast cancer. *Sci. Transl. Med.* **2019**, *11*, eaax9364. [[CrossRef](#)]
25. Mikulak, J.; Oriolo, F.; Bruni, E.; Roberto, A.; Colombo, F.S.; Villa, A.; Bosticardo, M.; Bortolomai, I.; Presti, E.L.; Meraviglia, S.; et al. Nkp46-expressing human gut-resident intraepithelial $V\delta 1$ T cell subpopulation exhibits high antitumor activity against colorectal cancer. *JCI Insight* **2019**, *4*, 125884. [[CrossRef](#)]
26. Foord, E.; Arruda, L.C.M.; Gaballa, A.; Klynning, C.; Uhlin, M. Characterization of ascites- and tumor-infiltrating $\gamma\delta$ T cells reveals distinct repertoires and a beneficial role in ovarian cancer. *Sci. Transl. Med.* **2021**, *13*, 0192. [[CrossRef](#)]
27. Pizzolato, G.; Kaminski, H.; Tosolini, M.; Franchini, D.-M.; Pont, F.; Martins, F.; Valle, C.; Labourdette, D.; Cadot, S.; Quillet-Mary, A.; et al. Single-cell RNA sequencing unveils the shared and the distinct cytotoxic hallmarks of human TCRV $\delta 1$ and TCRV $\delta 2$ $\gamma\delta$ T lymphocytes. *Proc. Natl. Acad. Sci. USA* **2019**, *116*, 11906–11915. [[CrossRef](#)]
28. Cerapio, J.-P.; Perrier, M.; Balança, C.-C.; Gravelle, P.; Pont, F.; Devaud, C.; Franchini, D.-M.; Féliu, V.; Tosolini, M.; Valle, C.; et al. Phased differentiation of $\gamma\delta$ T and T CD8 tumor-infiltrating lymphocytes revealed by single-cell transcriptomics of human cancers. *OncolImmunology* **2021**, *10*, 1939518. [[CrossRef](#)]
29. Aoki, T.; Chong, L.C.; Takata, K.; Milne, K.; Hav, M.; Colombo, A.; Chavez, E.A.; Nissen, M.; Wang, X.; Miyata-Takata, T.; et al. Single-Cell Transcriptome Analysis Reveals Disease-Defining T-cell Subsets in the Tumor Microenvironment of Classic Hodgkin Lymphoma. *Cancer Discov.* **2019**, *10*, 406–421. [[CrossRef](#)]
30. Cillo, A.R.; Kürten, C.H.; Tabib, T.; Qi, Z.; Onkar, S.; Wang, T.; Liu, A.; Duvvuri, U.; Kim, S.; Soose, R.J.; et al. Immune Landscape of Viral- and Carcinogen-Driven Head and Neck Cancer. *Immuni* **2020**, *52*, 183–199.e21. [[CrossRef](#)]
31. Stuart, T.; Butler, A.; Hoffman, P.; Hafemeister, C.; Papalexi, E.; Mauck, W.M., III; Hao, Y.; Stoeckius, M.; Smibert, P.; Satija, R. Comprehensive Integration of Single-Cell Data. *Cell* **2019**, *177*, 1888–1902. [[CrossRef](#)] [[PubMed](#)]
32. McInnes, L.; Healy, J. UMAP: Uniform Manifold Approximation and Projection for Dimension Reduction. Available online: <https://arxiv.org/abs/1802.03426> (accessed on 12 October 2021).
33. Pont, F.; Tosolini, M.; Fournié, J.J. Single-Cell Signature Explorer for comprehensive visualization of single cell signatures across scRNA-seq datasets. *Nucleic Acids Res.* **2019**, *47*, e133. [[CrossRef](#)] [[PubMed](#)]
34. Pont, F.; Tosolini, M.; Gao, Q.; Perrier, M.; Madrid-Mencía, M.; Huang, T.S.; Neuvial, P.; Ayyoub, M.; Nazor, K.; Fournié, J.-J. Single-Cell Virtual Cytometer allows user-friendly and versatile analysis and visualization of multimodal single cell RNAseq datasets. *NAR Genom. Bioinform.* **2020**, *2*, lqaa025. [[CrossRef](#)] [[PubMed](#)]
35. Chihara, N.; Madi, A.; Kondo, T.; Zhang, H.; Acharya, N.; Singer, M.; Nyman, J.; Marjanovic, N.D.; Kowalczyk, M.S.; Wang, C.; et al. Induction and transcriptional regulation of the co-inhibitory gene module in T cells. *Nat. Cell Biol.* **2018**, *558*, 454–459. [[CrossRef](#)]
36. Alfei, F.; Kanev, K.; Hofmann, M.; Wu, M.; Ghoneim, H.E.; Roelli, P.; Utschneider, D.T.; Von Hoesslin, M.; Cullen, J.G.; Fan, Y.; et al. TOX reinforces the phenotype and longevity of exhausted T cells in chronic viral infection. *Nature* **2019**, *571*, 265–269. [[CrossRef](#)]
37. Khan, O.; Giles, J.R.; McDonald, S.; Manne, S.; Ngiow, S.F.; Patel, K.P.; Werner, M.T.; Huang, A.C.; Alexander, K.A.; Wu, J.E.; et al. TOX transcriptionally and epigenetically programs CD8+ T cell exhaustion. *Nature* **2019**, *571*, 211–218. [[CrossRef](#)]
38. Tosolini, M.; Alkans, C.; Pont, F.; Ycart, B.; Fournié, J.-J. Large-scale microarray profiling reveals four stages of immune escape in non-Hodgkin lymphomas. *OncolImmunology* **2016**, *5*, e1188246. [[CrossRef](#)]

39. Balança, C.-C.; Scarlata, C.-M.; Michelas, M.; Devaud, C.; Sarradin, V.; Franchet, C.; Gomez, C.M.; Gomez-Roca, C.; Tosolini, M.; Heaugwane, D.; et al. Dual Relief of T-lymphocyte Proliferation and Effector Function Underlies Response to PD-1 Blockade in Epithelial Malignancies. *Cancer Immunol. Res.* **2020**, *8*, 869–882. [[CrossRef](#)]
40. Kumar, B.V.; Ma, W.; Miron, M.; Granot, T.; Guyer, R.S.; Carpenter, D.J.; Senda, T.; Sun, X.; Ho, S.-H.; Lerner, H.; et al. Human Tissue-Resident Memory T Cells Are Defined by Core Transcriptional and Functional Signatures in Lymphoid and Mucosal Sites. *Cell Rep.* **2017**, *20*, 2921–2934. [[CrossRef](#)]
41. Wu, T.D.; Madireddi, S.; de Almeida, P.E.; Banchereau, R.; Chen, Y.-J.J.; Chitre, A.S.; Chiang, E.Y.; Iftikhar, H.; O’Gorman, W.E.; Au-Yeung, A.; et al. Peripheral T cell expansion predicts tumour infiltration and clinical response. *Nat. Cell Biol.* **2020**, *579*, 274–278. [[CrossRef](#)]
42. Alpert, A.; Moore, L.S.; Dubovik, T.; Shen-Orr, S.S. Alignment of single-cell trajectories to compare cellular expression dynamics. *Nat. Methods* **2018**, *15*, 267–270. [[CrossRef](#)]
43. Trapnell, C.; Cacchiarelli, D.; Grimsby, J.; Pokharel, P.; Li, S.; Morse, M.; Lennon, N.J.; Livak, K.J.; Mikkelsen, T.S.; Rinn, J.L. The dynamics and regulators of cell fate decisions are revealed by pseudotemporal ordering of single cells. *Nat. Biotechnol.* **2014**, *32*, 381–386. [[CrossRef](#)]
44. Berge, K.V.D.; de Bézieux, H.R.; Street, K.; Saelens, W.; Cannoodt, R.; Saeys, Y.; Dudoit, S.; Clement, L. Trajectory-based differential expression analysis for single-cell sequencing data. *Nat. Commun.* **2020**, *11*, 1–13. [[CrossRef](#)]
45. Lo Presti, E.; Dieli, F. and Meraviglia, S. Lymphopenia in COVID-19: Gammadelta T Cells-Based Therapeutic Opportunities. *Vaccines (Basel)* **2021**, *9*, 562. [[CrossRef](#)]
46. Caron, J.; Ridgley, L.A.; Bodman-Smith, M. How to Train Your Dragon: Harnessing Gamma Delta T Cells Antiviral Functions and Trained Immunity in a Pandemic Era. *Front. Immunol.* **2021**, *12*, 666983. [[CrossRef](#)]
47. Yazdanifar, M.; Mashkour, N.; Bertaina, A. Making a case for using $\gamma\delta$ T cells against SARS-CoV-2. *Crit. Rev. Microbiol.* **2020**, *46*, 689–702. [[CrossRef](#)]
48. Orumaa, K.; Dunne, M.R. The role of unconventional T cells in COVID-19. *Ir. J. Med. Sci.* **2021**, 1–10. [[CrossRef](#)]
49. Lei, L.; Qian, H.; Yang, X.; Zhang, X.; Zhang, D.; Dai, T.; Guo, R.; Shi, L.; Cheng, Y.; Zhang, B.; et al. The phenotypic changes of $\gamma\delta$ T cells in COVID-19 patients. *J. Cell. Mol. Med.* **2020**, *24*, 11603–11606. [[CrossRef](#)]
50. Moratto, D.; Chiarini, M.; Giustini, V.; Serana, F.; Magro, P.; Roccaro, A.M.; Imberti, L.; Castelli, F.; Notarangelo, L.D.; Quiros-Roldan, E. Flow Cytometry Identifies Risk Factors and Dynamic Changes in Patients with COVID-19. *J. Clin. Immunol.* **2020**, *40*, 970–973. [[CrossRef](#)]
51. Carter, M.J.; Fish, M.; Jennings, A.; Doores, K.J.; Wellman, P.; Seow, J.; Acors, S.; Graham, C.; Timms, E.; Kenny, J.; et al. Peripheral immunophenotypes in children with multisystem inflammatory syndrome associated with SARS-CoV-2 infection. *Nat. Med.* **2020**, *26*, 1701–1707. [[CrossRef](#)]
52. Guo, C.; Li, B.; Ma, H.; Wang, X.; Cai, P.; Yu, Q.; Zhu, L.; Jin, L.; Jiang, C.; Fang, J.; et al. Single-cell analysis of two severe COVID-19 patients reveals a monocyte-associated and tocilizumab-responding cytokine storm. *Nat. Commun.* **2020**, *11*, 1–11. [[CrossRef](#)]
53. Xu, X.; Han, M.; Li, T.; Sun, W.; Wang, D.; Fu, B.; Zhou, Y.; Zheng, X.; Yang, Y.; Li, X.; et al. Effective treatment of severe COVID-19 patients with tocilizumab. *Proc. Natl. Acad. Sci. USA* **2020**, *117*, 10970–10975. [[CrossRef](#)]
54. Presti, E.L.; Corsale, A.M.; Dieli, F.; Meraviglia, S. $\gamma\delta$ cell-based immunotherapy for cancer. *Expert Opin. Biol. Ther.* **2019**, *19*, 887–895. [[CrossRef](#)]
55. Simoni, Y.; Becht, E.; Fehlings, M.G.; Loh, C.Y.; Koo, S.-L.; Teng, K.W.W.; Yeong, J.P.S.; Nahar, R.; Zhang, T.; Kared, H.; et al. Bystander CD8⁺ T cells are abundant and phenotypically distinct in human tumour infiltrates. *Nature* **2018**, *557*, 575–579. [[CrossRef](#)]
56. Oliveira, G.; Stromhaug, K.; Klaeger, S.; Kula, T.; Frederick, D.T.; Le, P.M.; Forman, J.; Huang, T.; Li, S.; Zhang, W.; et al. Phenotype, specificity and avidity of antitumour CD8⁺ T cells in melanoma. *Nat. Cell Biol.* **2021**, *596*, 119–125. [[CrossRef](#)]